

Chapter III.7

X-ray free-electron-lasers

Eduard Prat

Paul Scherrer Institute, Villigen, Switzerland

X-ray free-electron laser (FEL) facilities are unique tools providing extremely brilliant X-rays that allow the observation of matter on the scale of atomic processes. In this chapter we will qualitatively explain some fundamental concepts related to undulator and FEL radiation and we will describe the X-ray FEL facilities, including the typical layout, some basic concepts about electron beam dynamics and properties, and current facilities.

X-ray free-electron lasers (FELs) are unique instruments to observe matter on spatial and time scales of atomic processes. They can address fundamental research questions across the disciplines of physics, chemistry, materials and life sciences. The figure of merit of many X-ray experiments and therefore used to compare different radiation sources is the brilliance or spectral brightness. The peak brilliance is defined as the number of photons emitted by the source per unit of time into a unit of solid angle, per unit of emitting surface, and into a unit bandwidth of frequencies around the central one. The unit for peak brilliance is [photons / s / mm² / mrad² / 0.1% (BW)]. Figure III.7.1 shows the historical evolution of peak brilliance for X-rays. X-ray FELs are the most brilliant sources: they provide peak brilliances much higher than synchrotron facilities (e.g., about 10 orders of magnitude higher than third-generation synchrotrons). This is thanks to the increased pulse energies, shorter pulse durations, and lower bandwidths.

Here, we will first qualitatively describe some basic concepts about undulator radiation and the FEL process. Afterwards we will explain X-ray FEL facilities, namely the standard layout, some fundamental concepts related to electron beam dynamics and properties, and a list of the current facilities presently in operation around the globe. The chapter is based on the seminar on FELs given at the JUAS and has been inspired by the proceedings of the lectures on *Synchrotron light circular machines and FELs* given at the course *Introduction to Accelerator Physics* at the CERN Accelerator School [1]. We recommend Refs. [2–5] for further and deeper reading.

III.7.1 Basic FEL physics principles

III.7.1.1 Undulator radiation

Undulators are devices which consist of a periodic structure of dipole magnets with alternating polarity. The undulator is defined by the number of periods or bending magnets N and by the undulator period λ_u , the latter with typical values of a few centimeters. Figure III.7.2 shows a sketch of an undulator and

This chapter should be cited as: X-ray free-electron-lasers, E. Prat, DOI: [10.23730/CYRSP-2024-003.2057](https://doi.org/10.23730/CYRSP-2024-003.2057), in: Proceedings of the Joint Universities Accelerator School (JUAS): Courses and exercises, E. Métral (ed.), CERN Yellow Reports: School Proceedings, CERN-2024-003, DOI: [10.23730/CYRSP-2024-003](https://doi.org/10.23730/CYRSP-2024-003), p. 2057. © CERN, 2024. Published by CERN under the [Creative Commons Attribution 4.0 license](https://creativecommons.org/licenses/by/4.0/).

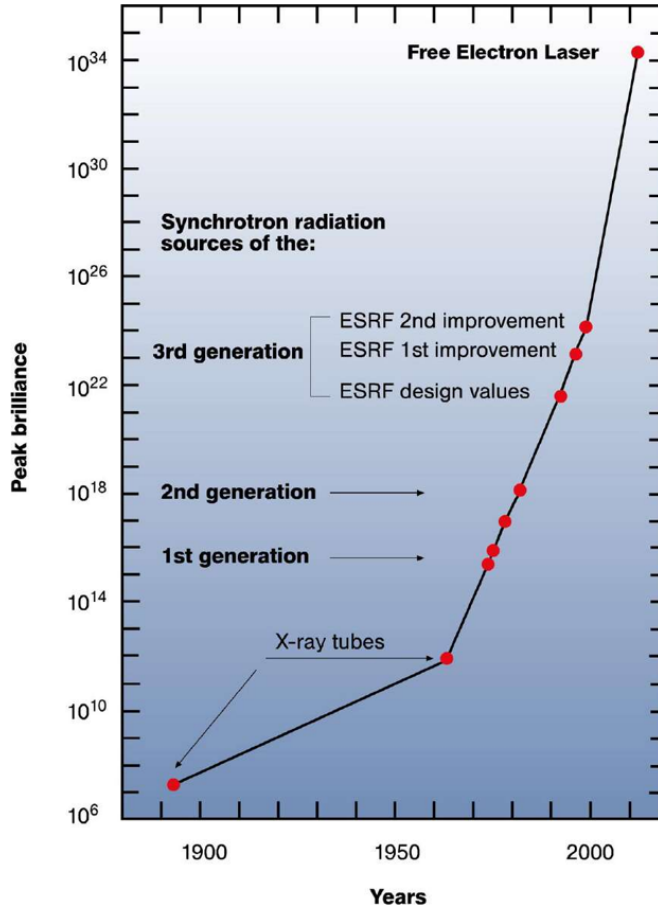


Fig. III.7.1: Evolution of peak brilliance of X-ray sources. Image taken from Ref. [6].

its working principle. The on-axis magnetic field of a standard planar undulator is non-zero only in the vertical (horizontal) direction, assuming the motion of the electron beam is in the horizontal (vertical) plane, and it can be expressed as

$$B_y = B_0 \cos k_u z \quad , \quad (\text{III.7.1})$$

where B_0 is the peak magnetic field, $k_u = 2\pi/\lambda_u$ is the wave number of the undulator, and z is the longitudinal coordinate along the undulator. The undulator field is normally described by the undulator parameter K :

$$K = \frac{eB_0}{mck_u} \quad , \quad (\text{III.7.2})$$

where e is the electron charge, m is the electron rest mass, and c is the speed of light. K is dimensionless and has typical values around 1. In practical units it can be expressed as $K \approx 0.93 B_0(\text{T})\lambda_u(\text{cm})$.

III.7.1.1.1 Motion in the undulator

The motion of an electron traveling through an undulator is defined by the Lorentz force: $\vec{F} = e(\vec{v} \times \vec{B})$. Here, \vec{v} is the velocity of the electron, which is dominant in the longitudinal direction z and can be approximated as $v_z = \beta_z c$. Assuming that the magnetic field \vec{B} is dominant in the vertical plane y , the

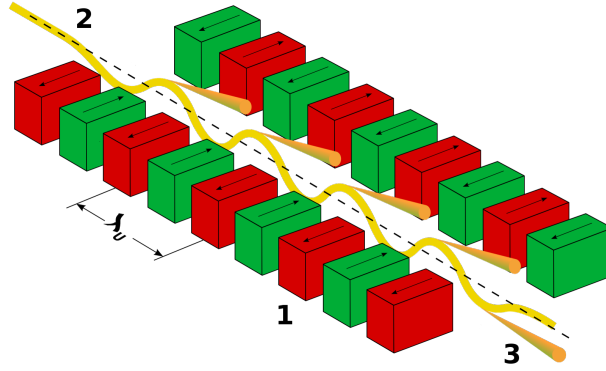


Fig. III.7.2: Sketch of an undulator and its working principle. 1: magnets with alternating polarity, 2: the yellow line indicates the electron beam trajectory entering from the upper left; 3: the orange cones show the synchrotron radiation produced in the forward direction. Image from Bastian Holst [7].

force will be dominant in the horizontal direction x (see Eq. III.7.1):

$$F_x = e(-v_z B_y) \approx -ec\beta_z B_0 \cos k_u z \quad . \quad (\text{III.7.3})$$

We know that the force is the derivative of the momentum over time, so we can write, considering that $\gamma^2 = 1/(1 - \beta^2)$ is constant (since the energy is conserved during motion under the influence of a magnetic field) that

$$F_x = \frac{dp_x}{dt} = \gamma mc \frac{d\beta_x}{dt} \quad . \quad (\text{III.7.4})$$

From the two previous equations we can derive, after some algebra, the transverse and longitudinal motion of the electrons in the undulator:

$$\beta_x = -\frac{K}{\gamma} \sin k_u z, \quad (\text{III.7.5})$$

$$\beta_z = 1 - \frac{1 + K^2/2}{2\gamma^2} + \frac{K^2}{4\gamma^2} \cos(2k_u z) = \langle \beta_z \rangle + \frac{K^2}{4\gamma^2} \cos(2k_u z) \quad , \quad (\text{III.7.6})$$

where $\langle \beta_z \rangle$ is the average longitudinal velocity over one undulator period relative to the speed of light. We observe that the longitudinal wiggle has twice the period than the transverse one. In the rest frame of the undulator, this results in an electron trajectory with a characteristic 8 shape.

III.7.1.1.2 Resonance condition

Figure III.7.3 shows a sketch useful to understand how to have constructive interference between the radiation emitted by the same electron at different locations in the undulator. To achieve this constructive interference, the electron must slip back by exactly one radiation wavelength λ (or an integer multiple of it) over one undulator period. In order to fulfill this condition, under an arbitrary emission direction θ , the radiation wavelength (or an integer multiple n of it) has to be exactly $R_w - \lambda_u \cos \theta$, where R_w is the radius of the wavefront emitted by the electron one undulator period before.

The radius R_w can be obtained as $R_w = cT$, where T is the time needed for the electron to move

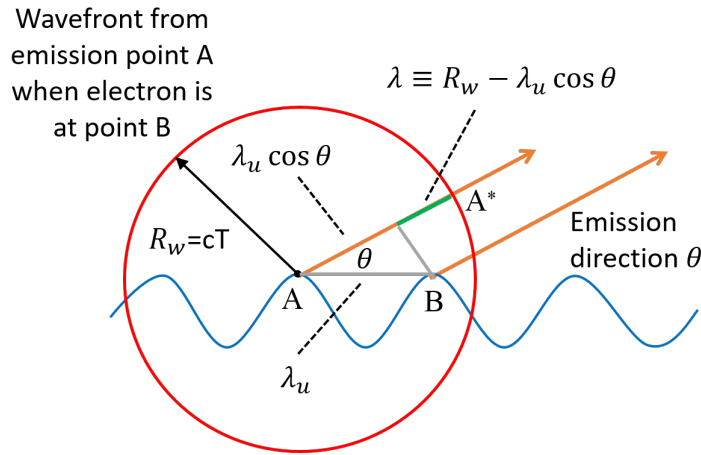


Fig. III.7.3: Sketch to show the condition for constructive interference between photons emitted at different locations in the undulator. The blue line shows the trajectory of the electron within the undulator. At point A the electron emits radiation in all directions. When the electron has moved by one undulator period and it is at point B , the wavefront emitted from A has a radius of R_w . This wavefront is indicated by the red circle, with the point A^* indicating the emission in the direction θ . At that moment the electron emits an identical wavefront from point B . After certain time (i.e., in the far field), the distance between the two wavefronts in the direction θ settles to a constant value indicated by the length of the green line in the sketch. For a constructive interference between both wavefronts this distance has to be exactly the radiation wavelength λ (or an integer multiple n of it); i.e., $n\lambda = R_w - \lambda_u \cos \theta$. Image courtesy of Sven Reiche.

by one undulator period; i.e.; $T = (\lambda_u / (\langle \beta_z \rangle c))$. From the expression of $\langle \beta_z \rangle$ in Eq. III.7.6, we have:

$$R_w = cT = c \frac{\lambda_u}{\langle \beta_z \rangle c} = \lambda_u \frac{1}{1 - \frac{1+K^2/2}{2\gamma^2}} \approx \lambda_u \left(1 + \frac{1+K^2/2}{2\gamma^2} \right) . \quad (\text{III.7.7})$$

Moreover, for a small emission angle θ , we can write $\lambda_u \cos \theta \approx \lambda_u (1 - \theta^2/2)$. If we put this together with $n\lambda = R_w - \lambda_u \cos \theta$ we find the following condition:

$$\lambda = \frac{\lambda_u}{2n\gamma^2} \left(1 + \frac{K^2}{2} + \theta^2\gamma^2 \right) . \quad (\text{III.7.8})$$

In the forward direction ($\theta = 0$) we obtain the so-called resonance condition:

$$\lambda_R = \frac{\lambda_u}{2n\gamma^2} \left(1 + \frac{K^2}{2} \right) . \quad (\text{III.7.9})$$

We observe that the wavelength increases with θ^2 , i.e., it gets longer as we move away from the axis. The resonance condition shows that the radiation wavelengths become shorter than the undulator period by a factor proportional to $1/\gamma^2$. We can also observe that the radiation wavelength increases with the magnetic field, parameterized by K .

An important implication of the resonance condition is that the undulator radiation wavelength can be tuned: it can be controlled by either changing the electron beam energy ($E_e \propto \gamma$) or by varying

the undulator parameters (the period λ_u or the magnetic field K). As an example for the SwissFEL [8] case and for the fundamental radiation ($n = 1$), an undulator period of 15 mm, a K -value of 1.2 and an energy of 5.8 GeV gives a radiation wavelength of 0.1 nm.

III.7.1.2 FEL radiation

The FEL is a circular runaway process consisting in a simultaneous growth of the radiation field, the electron beam energy modulation, and the electron beam density modulation (also called microbunching). The FEL process starts with an initial radiation field, which in the standard FEL configuration is associated to the spontaneous undulator radiation generated by the electron beam. This initial field induces an energy modulation to the electron beam with a period equal to the radiation wavelength λ . The energy modulation is then converted to density modulation within the radiation wavelength λ . This microbunching results in an increase of the emitted radiation due to an increased degree of coherence. This, in turn, contributes again to enhance the energy modulation, and so on.

The transverse oscillation of the electrons within the undulator allows the coupling between the electron beam and the co-propagating field. The energy transfer between an electron and the photon is proportional to $\vec{v}_\perp \vec{E}$, where \vec{v}_\perp is the transverse velocity of the electron and \vec{E} is the radiation field. A single electron will move either with or against the field line, losing or gaining energy with respect to the photon depending on the sign of the product $\vec{v}_\perp \vec{E}$. It can be demonstrated that, in the constructive interference condition, i.e., when the resonance condition (Eq. III.7.9) is fulfilled, the direction of energy transfer remains constant over many undulator periods. For instance, after half an undulator period the radiation field has slipped half a wavelength, both velocity and field have changed sign and the direction of energy transfer stays the same.

The energy change of an electron with the longitudinal position in the undulator z can be calculated as follows:

$$\frac{d\gamma}{dz} = \frac{-ef_c K}{2\gamma} \frac{E_0}{mc^2} \sin \phi \quad , \quad (\text{III.7.10})$$

where f_c is the so-called coupling factor (with values around 0.9 for a planar undulator), E_0 is the initial peak radiation field, and ϕ is the phase within one wavelength. From the above expression it is clear that electrons with positive phase lose energy, while electrons with negative phases will gain energy. This will cause an energy modulation of the electron beam.

Electrons gaining energy will move faster ($d\phi/dz > 0$), while electrons losing energy will fall back ($d\phi/dz < 0$). For small energy deviations $\Delta\gamma$ the following expression can be derived:

$$\frac{d\phi}{dz} = 2k_u \frac{\Delta\gamma}{\gamma_r} \quad , \quad (\text{III.7.11})$$

where γ_r corresponds to the Lorentz factor that fulfills the resonance condition (Eq. III.7.9). Because of this effect the electrons will move together, they will be packed in a small fraction of the wavelength. In other words, the energy modulation will cause a density modulation or microbunching.

With the help of Fig. III.7.4 we can understand how the energy modulation and microbunching are generated. The radiation wavelength is normally much shorter than the bunch length, so at the beginning the electrons are randomly spread out over all phases (see Fig. III.7.4.1). Following Eq. III.7.10 the

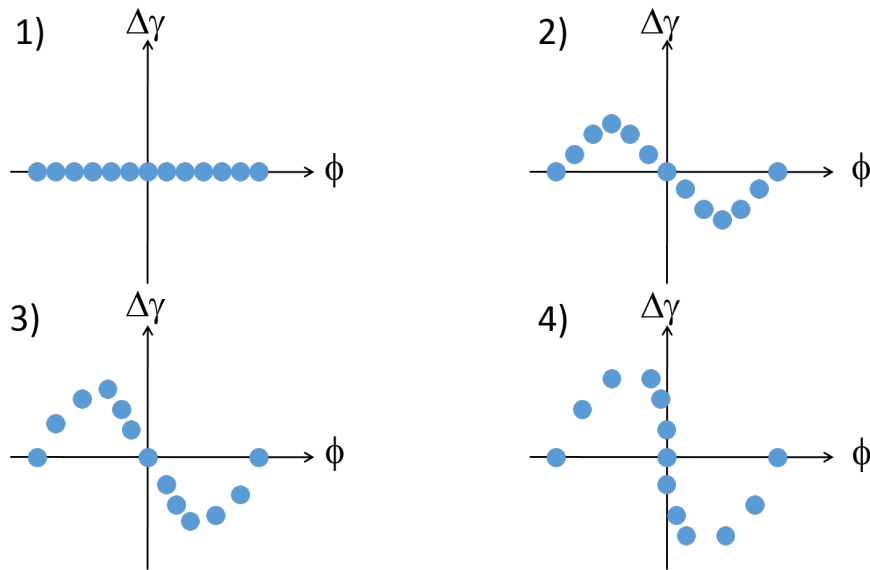


Fig. III.7.4: Longitudinal phase space of the electrons (symbolized with blue circles) at different stages: 1) no energy or density modulation, 2) initial energy modulation, 3) enhanced energy modulation and initial density modulation, 4) enhanced density modulation (microbunching). See text for more details. Image courtesy: Sven Reiche.

electrons will start to modulate in energy (Fig. III.7.4.2). After being modulated in energy they start to also modulate in density according to Eq. III.7.11 (Fig. III.7.4.3) until the beam is highly bunched (Fig. III.7.4.4).

Figure III.7.5 shows the generic FEL amplification process; i.e. how the FEL radiation power evolves along the undulator line. The undulator length is displayed in units of gain length L_g , defined as the required distance so that the power increases by a factor of e (in the exponential regime). We distinguish different regimes. At the startup there is a lethargy where the power does not grow. This corresponds to the time until some microbunching has been formed. After the lethargy there is the amplification regime in which the FEL power grows exponentially. The FEL process finishes with saturation. At this stage the microbunching has reached its maximum. Beyond saturation there is a continuous exchange of energy between electron beam and radiation beam and the FEL power stays rather constant.

III.7.1.2.1 FEL modes

The FEL can start either with the spontaneous undulator radiation generated by the electron beam or with an external radiation field. The first case, which is the standard FEL configuration, is called Self-Amplified Spontaneous Emission (SASE) FEL [9, 10]. The second case is referred to as seeded FEL. Figure III.7.6 shows a schematic layout of the SASE and seeded FEL options.

In SASE FELs, the electron beam travels through the undulator to generate the output radiation. The FEL process starts with the broadband signal of the spontaneous radiation, also called shot noise. SASE-FEL radiation is almost coherent in the transverse direction but not in the longitudinal one. Due to the lack of full longitudinal coherence, the spectrum and time profile contain several modes or spikes

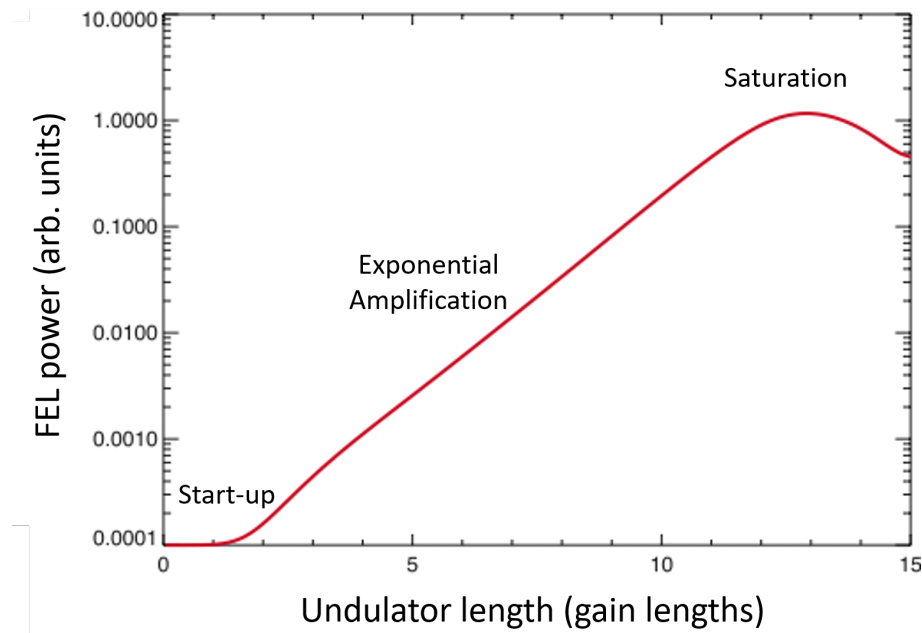


Fig. III.7.5: FEL power along the undulator. The vertical scale is logarithmic. Image courtesy: Sven Reiche.

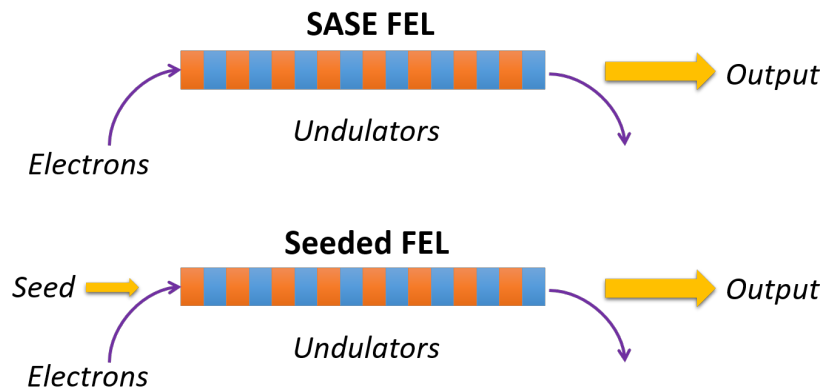


Fig. III.7.6: Schematic layouts of SASE and seeded-FEL modes. Image courtesy: Sven Reiche.

(a perfectly coherent pulse would only contain one mode in time and spectral domain). The FEL pulse duration t_b corresponds to the spike width in the spectrum $1/t_b$, while the time duration of a single spike in time profile t_c corresponds to the width of the full spectrum $1/t_c$. The bandwidth of the SASE-FEL radiation is of the order of the Pierce parameter (see later), with typical values for X-ray FEL facilities varying between 10^{-4} and 10^{-3} . Most of the X-ray FEL facilities are based on the SASE mechanism due to its simplicity and the technical complexity associated with seeded FELs.

In seeded FELs, the input of the undulator is not only the electron beam but also a seed signal, which is amplified within the undulator. The power of the seed has to be larger than the shot noise power

of the electron beam, otherwise the shot noise will be amplified. The output radiation will resemble the characteristics of the seed. For example, if the seed has a single mode in spectrum and time, the output radiation will also consist of a single mode. Seeding is used to improve the longitudinal coherence or to reduce the bandwidth of SASE-FELs. Fully coherent pulses can be obtained with the seeded-FEL process. There are various seeding methods. One possibility is to use the self-seeding mechanism [11, 12]: first, standard SASE-FEL radiation is produced in a first undulator section, then a radiation monochromator reduces the bandwidth of the SASE pulses, finally the monochromatic signal is used as a seed in a second amplification stage. Another option is to employ external lasers. Here it is possible to seed directly with a high-harmonic generation source [13] or to use more complicated layouts with modulators and chicanes such as in the high-gain harmonic generation [14] or the echo-enabled harmonic generation [15] schemes. Self-seeding has been proven to work for both soft and hard X-rays [16, 17], while external seeding using the HGHG and EEHG schemes have reached wavelengths of few nanometers, entering the soft X-ray regime [18, 19].

The peak brilliance shown in Fig. III.7.1 is for SASE-FELs. Seeded-FELs have demonstrated the possibility to reduce the bandwidth of SASE-FELs and therefore to increase the brilliance by an additional factor of 10–100 [16, 17].

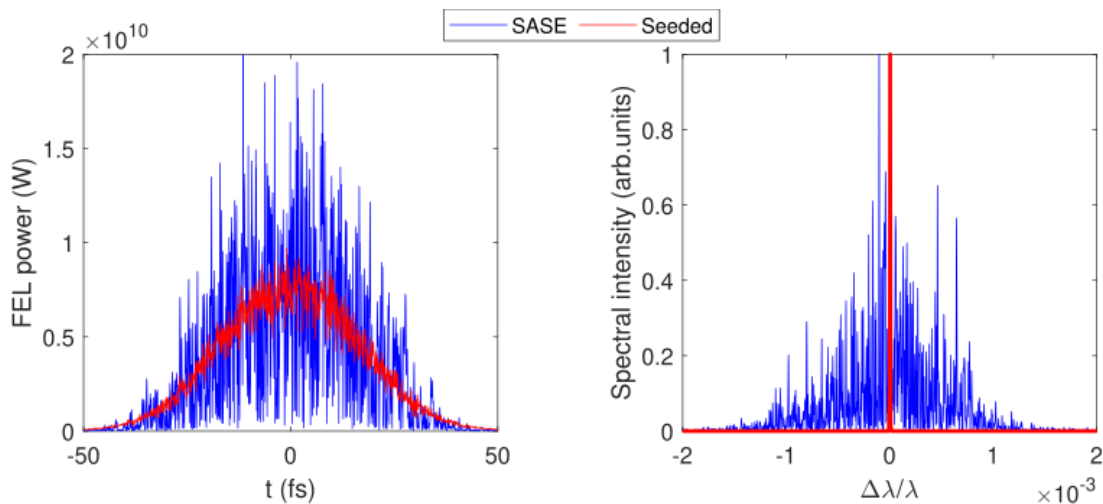


Fig. III.7.7: Simulated power profile (left) and spectrum normalized to maximum intensity (right) of a SASE and a seeded FEL for a radiation wavelength of 0.1 nm.

Figure III.7.7 shows a simulated power time profile and spectrum of a SASE and a seeded FEL at saturation for a radiation wavelength of 0.1 nm. In the seeded case, we consider a fully coherent initial field with a power of 1 MW. The rest of the simulation parameters are identical for both cases and correspond to the SwissFEL case. The simulations have been done with the code Genesis [20]. As observed in the figure, the SASE FEL has a spiky structure with multiple modes in both time and spectral domains, while the seeded FEL contains a single spike in both domains and the bandwidth is much smaller than for the SASE case.

III.7.1.2.2 FEL performance and electron beam requirements

The Pierce parameter ρ is a fundamental quantity to characterize the FEL process and performance:

$$\rho = \frac{1}{\gamma_r} \left[\left(\frac{f_c K}{4k_u \sigma_t} \right)^2 \frac{I}{2I_A} \right]^{1/3}, \quad (\text{III.7.12})$$

where I is the electron beam peak current, σ_t is the transverse electron beam size ($\sigma_t = \sqrt{\sigma_x \sigma_y}$), and I_A is the Alfvén current (≈ 17 kA). The Pierce parameter has typical values between 10^{-4} and 10^{-3} for X-ray FELs.

From 1D theory, the FEL power, the FEL gain length, and the relative bandwidth (in terms of angular frequency ω) can be obtained as [10]:

$$P = \rho P_e, \quad L_g = \frac{\lambda_u}{4\pi\sqrt{3}\rho}, \quad \frac{\Delta\omega}{\omega} = 2\rho, \quad (\text{III.7.13})$$

where P_e is the power of the electron beam. A better FEL performance, i.e., higher powers and shorter gain lengths, can be obtained for larger values of the Pierce parameter, although at the expense of a larger bandwidth. Considering Eq. III.7.12 this means that, besides aiming for larger undulator fields K (which require higher electron beam energies for the same wavelength, see Eq. III.7.9), the electron beam must have large peak current and small transverse beam size.

Moreover, we have to consider that only electrons within the FEL bandwidth can contribute to the FEL gain. Consequently, the relative energy spread of the electron beam needs to be smaller than the ρ parameter for an efficient FEL amplification, i.e.:

$$\frac{\sigma_\gamma}{\gamma} < \rho. \quad (\text{III.7.14})$$

For X-rays, the relative energy spread must be smaller than 10^{-3} .

Finally, we have to consider effects related to the transverse emittance. The transverse emittance of the electron beam is the area in the transverse phase-space $u-u'$, where u refers to either x or y , occupied by the fraction of the beam distribution determined by its second-order moments. It can be obtained as $\varepsilon_u = \sqrt{\sigma_u^2 \sigma_u'^2 - \sigma_{uu'}^2}$, where σ_u' is the transverse divergence of the electron beam and $\sigma_{uu'}$ its transverse coupling term. On the photon side, the radiation emittance of the fundamental mode of the field is given by $\lambda/(4\pi)$ [21]. Electrons enclosed in this effective phase-space ellipse of the photons will radiate coherently into the fundamental radiation mode. Electrons outside this ellipse will emit into higher modes and will not contribute to the amplification of the fundamental mode. This sets the following limit to the transverse emittance of the electron beam: $\varepsilon_u \lesssim \frac{\lambda}{4\pi}$. In FELs it is customary to normalize the electron beam emittance with respect to the electron beam momentum p , resulting in the normalized emittance $\varepsilon_{n,u} = \frac{p}{mc} \varepsilon_u \approx \gamma \varepsilon_u$. Then, the above limit can be rewritten as

$$\frac{\varepsilon_{n,u}}{\gamma} \lesssim \frac{\lambda}{4\pi}. \quad (\text{III.7.15})$$

This condition implies that, for the X-ray regime, normalized emittances at the micrometer level or below

are required.

III.7.2 X-ray FEL facilities

The FEL process requires electron beams with large peak currents, small beam sizes, emittances and energy spreads. In other words, electron beams with high charge density in the 6D phase space are required for FELs. For X-rays, the electron beam needs to have an energy at the GeV level, a peak current at the kA level, a relative energy spread between 0.01 and 0.1%, normalized emittances at the micrometer level or below, and transverse beam sizes of a few tens of micrometers or smaller. There are currently no electron sources that can produce such bunches directly. Instead they have to be accelerated and compressed. State-of-the-art X-ray FEL facilities employ linear accelerators to provide the drive electron beam (circular accelerators are not capable of delivering the required electron beam properties, in particular not the high peak current).

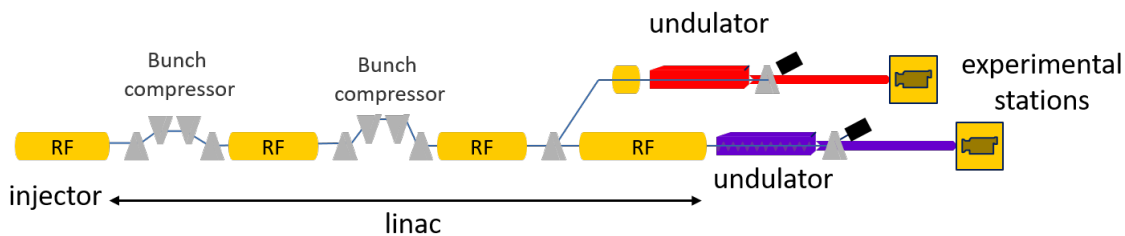


Fig. III.7.8: Sketch of a typical X-ray FEL facility.

III.7.2.1 Layout

Figure III.7.8 shows a schematic layout of a typical X-ray FEL. The facility can be separated into four main sections: the injector, where the high-brightness electrons are produced at relatively low energy and peak current; the linac, where the electrons are accelerated in RF sections and compressed in bunch compressors; the undulators, where the FEL process takes place; and the experimental stations, where the produced FEL radiation is used.

Most FELs use RF photoinjectors to generate high-brightness electron beams with energies of several MeV and peak currents of the order of 10 A or higher. Electrons are released via the photoelectric effect by a laser of a proper wavelength impinging on a photocathode mounted inside an RF gun. The cathode material is normally copper, although certain facilities such as European XFEL and SwissFEL operate with a cesium-telluride coating to profit from its higher quantum efficiency.

In the linac the electrons are accelerated to GeV energies and compressed to kA peak currents. Bunch compression is normally achieved in two or more sections within the linac. The accelerating frequency is in the GHz range. For instance, LCLS employs S-band technology (about 3 GHz) while SACLA and SwissFEL use C-band frequency (about 6 GHz). Higher frequencies permit acceleration of the beam over shorter distances and consequently result in a more compact linac. The linac can consist of normal-conducting RF cavities (“warm” technology) or superconducting ones (“cold” technology). In the latter case, many more pulses per second can be accelerated (e.g., 27 000 pulses per second at

the European XFEL with superconducting RF compared to 100 pulses per second at SwissFEL with normal-conducting RF).

The undulator beamline consists of several undulator modules, each of them with a length of a few meters and a period of a few centimeters. The space between two undulator modules, typically measuring around 1 m, is used for focusing the beam with quadrupole magnets as well as for diagnostic purposes. At the hard X-ray beamline of SwissFEL, for example, the undulator consists of 13 units, each of them with an undulator period of 15 mm, an undulator field parameter K tunable between 1 and 1.8, and a total length of 4 m. The interundulator section occupies 0.75 m. X-ray FEL facilities run one or several undulator beamlines, each of them serving multiple experimental stations.

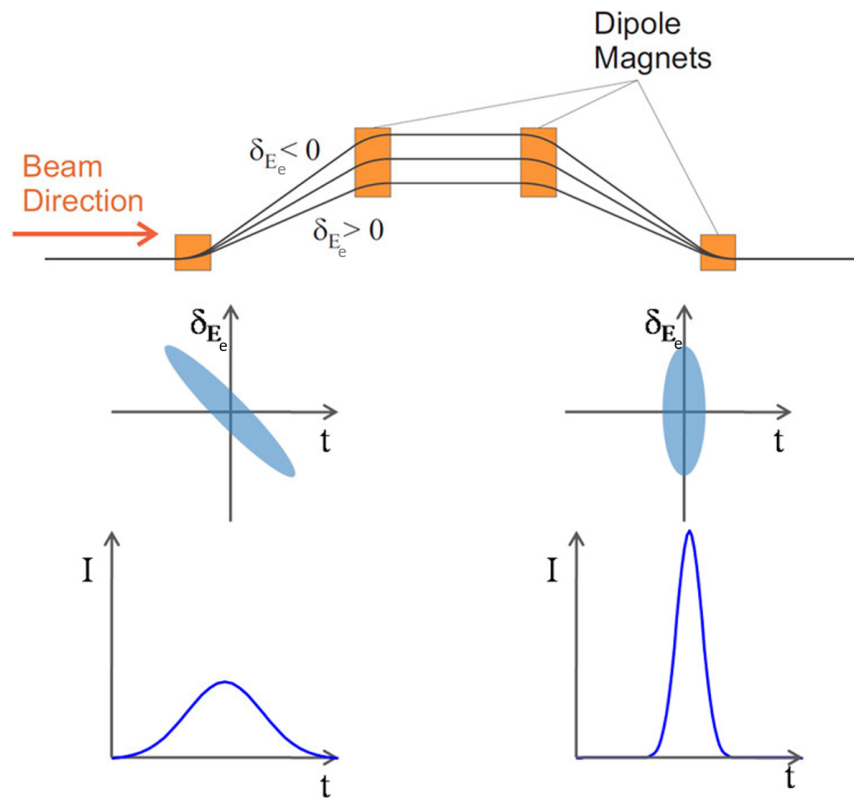


Fig. III.7.9: Principle of bunch compression. Top: trajectories of electrons with different energies (δ_{E_e} indicates relative energy variation) through a magnetic chicane of four dipole magnets. Center: longitudinal phase-space of the electron beam at the entrance (left) and the exit of the magnetic chicane. Bottom: current profile at the entrance (left) and exit (right) of the chicane. Image taken from [22].

III.7.2.2 Electron beam properties and dynamics

In linac-based X-ray FELs, which are single-pass machines, the electron beam properties are defined at the electron source, i.e., the RF photoinjector. The normalized emittances would ideally be preserved through the linac according to Liouville's theorem. However, Liouville's theorem will not be fulfilled and the beam emittances will be increased in the presence of some deteriorating stochastic effects such as nonlinear space-charge forces or emission of coherent synchrotron radiation. The main goal in designing and operating an FEL facility is to produce a high-brightness electron beam at the injector, accelerate it

and compress it in the linac while preserving its quality as much as possible.

The RF photoinjector produces electron beams with typical energies between 5 and 10 MeV, peak currents in the range 10–20 A, low normalized emittances (micrometer or below) and energy spreads at the level of a few keV. In the case of SwissFEL, the achieved injector parameters are a beam energy of 7.1 MeV, a peak current of 20 A, a normalized emittance of around 200 nm, and an energy spread of around 10 keV.

The emittance of the source is determined by three different components: intrinsic emittance of the cathode (mostly depending on the laser size at the cathode), space-charge forces, and RF field effects in the gun. The gun gradient is set as high as possible with available technology. In the SwissFEL example, the maximum RF field is 100 MV/m, resulting in the energy of 7.1 MeV at the gun exit quoted earlier. The gun is equipped with a solenoid magnet used to focus the electron beam. The laser spot size and the field generated by the gun solenoid are optimized to counteract the contributions of the intrinsic emittance (smaller for smaller spot size) and space charge (smaller for larger spot size) to the final emittance. This procedure is often referred to as emittance compensation [23].

Bunch compression follows a principle similar to FEL microbunching and is a two-stage process: First, the accelerating phases of some RF structures are tuned to imprint an energy chirp along the electron beam (i.e., a strong correlation between the energy and the longitudinal coordinate of the electrons along the bunch). Second, the beam is transported through a magnetic chicane, typically consisting of four bending magnets. Thanks to the energy dependence of the path along the chicane, the electron beam is compressed after the chicane. Figure III.7.9 illustrates how bunch compression works.

Bunch compression should be performed at suitable beam energies and currents to avoid beams with too high charge density, which would deteriorate the electron beam quality (in particular the emittance). Bunch compression is normally achieved in two or three stages along the linac. The first bunch compressor is typically at an energy of a few hundreds of MeV (300 MeV in the SwissFEL case) and the second or third when the energy already exceeds 1 GeV (2.1 GeV at SwissFEL). Each stage compresses the beam by a factor of around 10, resulting in a total bunch compression factor of around 100. At SwissFEL, the beam is compressed in the first bunch compressor to increase the peak current from 20 A to about 150 A, while the second bunch compressor further compresses the bunch to its final peak current of 2–3 kA.

In general, high charge densities give rise to strong electromagnetic fields generated by the electron bunches, which in turn affect the electrons within a bunch. Examples of such interactions include coherent synchrotron radiation in bunch compression chicanes, wakefields, and space-charge forces.

III.7.2.3 X-ray FEL projects around the world

The first FEL facility to reach wavelengths in the soft X-ray regime was FLASH at DESY (Germany) in 2007 [24]. Thanks to its superconducting RF technology, FLASH operates with repetition rates at the MHz level. In 2009, the Linac Coherent Light Source (LCLS) at SLAC (USA) was the first FEL facility to produce radiation in the hard X-ray regime, with wavelengths at the angstrom level [25]. Two years later, in 2011, SACLA at SPring-8 (Japan) came into operation, producing hard X-ray FEL light with a much more compact accelerator than LCLS [26]. In 2013, FERMI at Elettra Sincrotrone Trieste

Table III.7.1: Start of operation and main parameters of the hard X-ray FEL facilities presently operating worldwide [8, 25–29].

Name	Starting operation year	Energy (GeV)	Length (m)	Peak current (kA)	Normalized emittance (nm)
European XFEL (Germany)	2017	17.5	3400	5	< 600
LCLS (USA)	2009	14.3	3000	2.5–3.5	400
PAL XFEL (Korea)	2017	10	1100	2.5	550
SACLA (Japan)	2010	8.5	750	> 3	1000
SwissFEL (Switzerland)	2018	5.8	740	2	200

(Italy) was the first fully seeded FEL going into operation delivering soft X-rays [18]. In the last few years, three additional hard X-ray sources have started operation: PAL-XFEL at Pohang Accelerator Laboratory (South Korea) [27], the European XFEL at DESY (Germany) [28], employing, like FLASH, superconducting RF structures to run at MHz frequencies, and SwissFEL at PSI (Switzerland), the most compact and cost-effective hard X-ray facility to date, driven by a high-brightness and relatively low-energy electron beam [8]. Two more hard X-ray facilities are planned for the coming years: LCLS-II at SLAC (USA) and SHINE at SINAP (China), both of them adopting superconducting RF technology to be able to operate at MHz repetition rates. So far, all X-ray FEL facilities except FERMI are based on the SASE mechanism. However, most of these facilities have the option to produce seeded radiation via the self-seeding process [16, 17].

Table III.7.1 lists the start of operation and the main parameters (electron beam energy, facility length, electron beam current and normalized emittance) of the hard X-ray FEL facilities operating to date [8, 25–29]. The reported emittance values correspond to the core of the bunch (slice emittance) for all facilities except SACLA, for which the emittance value refers to the full bunch (projected emittance).

Acknowledgments

We would like to thank Sven Reiche and Thomas Schietinger for valuable comments and discussions that help to improve the quality and the language of the document.

References

- [1] E. Prat, Synchrotron light sources and X-ray free-electron-lasers, presented at the CERN Accelerator School, Chavannes de Bogis, Switzerland, 2021, doi:10.48550/arXiv.2107.09131.
- [2] K.-J. Kim, Z. Huang, and R. Lindberg, *Synchrotron radiation and free-electron lasers: Principles of coherent X-ray generation* (Cambridge Univ. Press, Cambridge, 2017), doi:10.1017/9781316677377.
- [3] Ph. Willmott, *An introduction to synchrotron radiation: Techniques and applications*, 2nd ed. (Wiley, Hoboken, New Jersey, 2019), doi:10.1002/9781119280453.
- [4] Eberhard Jaeschke *et al.* (Eds.), *Synchrotron light sources and free-electron lasers* (Springer, Cham, 2014), doi:10.1007/978-3-319-04507-8.

- [5] C. Pellegrini, A. Marinelli and S. Reiche, The physics of x-ray free-electron lasers, *Rev. Mod. Phys.* **88** (2016) 015006, doi:[10.1103/RevModPhys.88.015006](https://doi.org/10.1103/RevModPhys.88.015006).
- [6] M. Marklund and P.K. Shukla, Nonlinear collective effects in photon-photon and photon-plasma interactions, *Rev. Mod. Phys.* **78** (2006) 591–640, doi:[10.1103/revmodphys.78.591](https://doi.org/10.1103/revmodphys.78.591).
- [7] Wikimedia Commons contributors, *File:Undulator.png*, (Wikimedia Commons, 20 September 2020), accessed November 15, 2023, <https://commons.wikimedia.org/wiki/File:Undulator.png>.
- [8] E. Prat *et al.*, A compact and cost-effective hard X-ray free-electron laser driven by a high-brightness and low-energy electron beam, *Nature Photon.* **14** (2020) 748–754, doi:[10.1038/s41566-020-00712-8](https://doi.org/10.1038/s41566-020-00712-8).
- [9] A.M. Kondratenko and E.L. Saldin, Generation of coherent radiation by a relativistic electron beam in an undulator, *Part. Accel.* **10** (1980) 207–216, <https://cds.cern.ch/record/1107977>.
- [10] R. Bonifacio, C. Pellegrini and L.M. Narducci, Collective instabilities and high-gain regime in a free electron laser, *Opt. Commun.* **50** (1984) 373–378, doi:[10.1016/0030-4018\(84\)90105-6](https://doi.org/10.1016/0030-4018(84)90105-6).
- [11] J. Feldhaus *et al.*, Possible application of X-ray optical elements for reducing the spectral bandwidth of an X-ray SASE FEL, *Optics Comm.* **140** (1997) 341–352, doi:[10.1016/s0030-4018\(97\)00163-6](https://doi.org/10.1016/s0030-4018(97)00163-6).
- [12] E.L. Saldin *et al.*, X-ray FEL with a meV bandwidth, *Nucl. Instrum. Meth. A* **475** (2001) 357–362, doi:[10.1016/s0168-9002\(01\)01539-x](https://doi.org/10.1016/s0168-9002(01)01539-x).
- [13] M. Ferray *et al.*, Multiple-harmonic conversion of 1064 nm radiation in rare gases, *J. Phys. B* **21** (1988) L31–L35, doi:[10.1088/0953-4075/21/3/001](https://doi.org/10.1088/0953-4075/21/3/001).
- [14] L.H. Yu, Generation of intense UV radiation by subharmonically seeded single-pass free-electron lasers, *Phys. Rev. A* **44** (1991) 5178–5193, doi:[10.1103/physreva.44.5178](https://doi.org/10.1103/physreva.44.5178).
- [15] G. Stupakov, Using the beam-echo effect for generation of short-wavelength radiation, *Phys. Rev. Lett.* **102** (2009) 074801, doi:[10.1103/physrevlett.102.074801](https://doi.org/10.1103/physrevlett.102.074801).
- [16] D. Ratner *et al.*, Experimental demonstration of a soft X-ray self-seeded free-electron laser, *Phys. Rev. Lett.* **114** (2015) 054801, doi:[10.1103/physrevlett.114.054801](https://doi.org/10.1103/physrevlett.114.054801).
- [17] J. Amann *et al.*, Demonstration of self-seeding in a hard-X-ray free-electron laser, *Nature Photon.* **6** (2012) 693–698, doi:[10.1038/nphoton.2012.180](https://doi.org/10.1038/nphoton.2012.180).
- [18] E. Allaria *et al.*, Two-stage seeded soft-X-ray free-electron laser, *Nature Photon.* **7** (2013) 913–918, doi:[10.1038/nphoton.2013.277](https://doi.org/10.1038/nphoton.2013.277).
- [19] P.R. Ribič *et al.*, Coherent soft X-ray pulses from an echo-enabled harmonic generation free-electron laser, *Nature Photon.* **13** (2019) 555–561, doi:[10.1038/s41566-019-0427-1](https://doi.org/10.1038/s41566-019-0427-1).
- [20] S. Reiche, GENESIS 1.3: A fully 3D time-dependent FEL simulation code, *Nucl. Instrum. Meth. A* **429** (1999) 243–248, doi:[10.1016/S0168-9002\(99\)00114-X](https://doi.org/10.1016/S0168-9002(99)00114-X).
- [21] A.E. Siegman, *Lasers* (University Science Books, Melville, NY, 1986), <https://uscibooks.aip.org/books/lasers/>.
- [22] Paul Scherrer Institut, *Accelerators and beamlines*, accessed November 15, 2023, <https://www.psi.ch/en/swissfel/accelerator>.

- [23] L. Serafini and J.B. Rosenzweig, Envelope analysis of intense relativistic quasilaminar beams in RF photoinjectors: mA theory of emittance compensation, *Phys. Rev. E* **55** (1997) 7565–7590, [doi:10.1103/physreve.55.7565](https://doi.org/10.1103/physreve.55.7565).
- [24] W. Ackermann et al., Operation of a free-electron laser from the extreme ultraviolet to the water window, *Nature Photon.* **1** (2007) 336–342, [doi:10.1038/nphoton.2007.76](https://doi.org/10.1038/nphoton.2007.76).
- [25] P. Emma et al., First lasing and operation of an ångstrom-wavelength free-electron laser, *Nature Photon.* **4** (2010) 641–647, [doi:10.1038/nphoton.2010.176](https://doi.org/10.1038/nphoton.2010.176).
- [26] T. Ishikawa et al., A compact X-ray free-electron laser emitting in the sub-ångström region, *Nature Photon.* **6** (2012) 540–544, [doi:10.1038/nphoton.2012.141](https://doi.org/10.1038/nphoton.2012.141).
- [27] H.-S. Kang et al., Hard X-ray free-electron laser with femtosecond-scale timing jitter, *Nature Photon.* **11** (2017) 708–713, [doi:10.1038/s41566-017-0029-8](https://doi.org/10.1038/s41566-017-0029-8).
- [28] W. Decking et al., A MHz-repetition-rate hard X-ray free-electron laser driven by a superconducting linear accelerator, *Nature Photon.* **14** (2020) 391–397, [doi:10.1038/s41566-020-0607-z](https://doi.org/10.1038/s41566-020-0607-z).
- [29] European X-Ray Free-Electron Laser Facility, *European XFEL in international comparison*, accessed November 15, 2023, https://www.xfel.eu/facility/comparison/index_eng.html.